

GoPRONTO: a Feedback-based Framework for Nonlinear Optimal Control

Lorenzo Sforni, Sara Spedicato, Ivano Notarnicola, Giuseppe Notarstefano

Abstract

We propose GoPRONTO, a first-order, feedback-based approach to solve nonlinear discrete-time optimal control problems. This method is a generalized first-order framework based on incorporating the original dynamics into a closed-loop system. By exploiting this feedback-based shooting, we are able to reinterpret the optimal control problem as the minimization of a cost function, depending on a state-input curve, whose gradient can be computed by resorting to a suitable costate equation. This convenient reformulation gives room for a collection of accelerated numerical optimal control schemes. To corroborate the theoretical results, numerical simulations on the optimal control of a train of inverted pendulum-on-cart systems are shown.

Index Terms

Numerical optimal control, nonlinear control systems, trajectory optimization, gradient methods.

I. INTRODUCTION

Nonlinear optimal control problems arise in a vast number of engineering applications in Automation and Robotics.

In this note, we focus on *direct methods* for the resolution of discrete-time optimal control problems. These methods are subclassified into two different categories: *simultaneous* and *sequential* (see [2]). In simultaneous approaches, both the controls and the states are treated as decision variables of the nonlinear program (NLP), obtained via, e.g., collocation or multiple

The authors are with the Department of Electrical, Electronic and Information Engineering, Alma Mater Studiorum - Università di Bologna, Bologna, Italy, `name.lastname@unibo.it`.

This result is part of a project that has received funding from the European Research Council (ERC) under the European Union's Horizon 2020 research and innovation programme (grant agreement No 638992 - OPT4SMART). A very preliminary version of the idea inspiring this work, customized for the distributed framework, is proposed in [1].

shooting methods from the original optimal control problem formulation. The NLP is then addressed solving directly the Karush-Kuhn-Tucker optimality conditions of the problem by Newton's type optimization algorithms like Sequential Quadratic Programming (SQP) [2] and Interior Point optimization (IP) [3], [4]. These methods have been implemented in a variety of toolboxes, e.g., [5]–[9]. While these approaches do not exhibit numerical instability issues coming from the integration of the dynamics, an important drawback is that, in general, the constraints describing the dynamics are satisfied only asymptotically. That is, suboptimal state-input curves do not satisfy the dynamics in general. Conversely, sequential approaches tackle the NLP in the reduced space of control variables only. Hence, at each iteration, the state trajectory is recovered by forward simulation of the system dynamics. A first-order sequential approach for the resolution of nonlinear optimal control problems is presented, e.g., in [10, Section 1.9]. The main limitation of sequential methods is their numerical instability in the forward simulation of (the possibly unstable) dynamics. This issue is overcome by the original sequential method *Projection Operator Newton Method for Trajectory Optimization (PRONTO)* [11]. In this work, through the use of a control feedback, the shooting map is stabilized and the optimal control problem is converted into an unconstrained one to which a Newton's method is applied. This approach has been successfully extended in a variety of scenarios [12]–[16]. The introduction of stabilizing controllers to handle unstable dynamics is considered also in the model predictive control literature, see, e.g., [17], [18]. Finally, optimal control problems have been also tackled via augmented Lagrangian approaches in [19].

The main contribution of this note is to provide a novel class of numerically-robust first-order algorithms for (offline) discrete-time optimal control termed GoPRONTO, short for Generalized first-Order PROjectionN operator method for Trajectory Optimization¹. In our approach we combine the introduction of a feedback system (projection operator) into the nonlinear optimal control problem with a gradient-based resolution strategy. Such innovative combination results into an optimization framework that enjoys several appealing features. Thanks to the introduction of the projection operator in the sequential optimization scheme, we achieve (i) numerical robustness, even when dealing with unstable dynamics, and (ii) dynamic feasibility, i.e., a state-input trajectory can be computed, at each iteration, via a closed-loop integration of the nonlinear dynamics. This property is of particular interest in the case of, e.g., unstable systems. From the

¹This acronym is chosen as a tribute to Hauser's PRONTO.

(open-loop) gradient method for optimal control in [10], our approach inherits the simplicity of implementation of the descent-direction search, namely a costate equation update. Finally, we show how GoPRONTO gives rise to several first-order optimization algorithms that can speed up the resolution of the optimal control problem. This simple and adaptable update rule makes GoPRONTO flexible enough to be extended to problems involving large-scale dynamics. As in other optimization domains with very-large decision variables, Newton’s methods are impracticable while first-order approaches are preferred.

The note unfolds as follows. The nonlinear optimal control problem is presented in Section II along with some preliminaries. In Section III we propose our methodology GoPRONTO in its steepest descent implementation. Accelerated versions of GoPRONTO are presented in Section IV. Some numerical simulations with a train of inverted pendulum-on-cart systems are given in Section V.

Notation: The vertical stack of x_1 and x_2 is denoted by $\text{col}(x_1, x_2) := [x_1^\top, x_2^\top]^\top$. Given $\ell : \mathbb{R}^n \times \mathbb{R}^m \rightarrow \mathbb{R}$, its (total) gradient at a given point (\bar{x}, \bar{u}) is $\nabla \ell(\bar{x}, \bar{u}) := \text{col}(\nabla_x \ell(\bar{x}, \bar{u}), \nabla_u \ell(\bar{x}, \bar{u}))$, where $\nabla_x \ell(\bar{x}, \bar{u})$ and $\nabla_u \ell(\bar{x}, \bar{u})$ are the partial derivative of ℓ with respect to the first and the second argument, respectively. Moreover, given $f : \mathbb{R}^n \rightarrow \mathbb{R}^m$, the gradient of f is $\nabla f(x) := [\nabla f_1(x) \dots \nabla f_m(x)] \in \mathbb{R}^{n \times m}$. For $T \in \mathbb{N}$, we define $[0, T] := \{0, 1, 2, \dots, T\}$. Given a symmetric, positive-definite matrix $Q \in \mathbb{R}^{n \times n}$, and $x \in \mathbb{R}^n$, we define the Q -norm of x as $\|x\|_Q = \sqrt{x^\top Q x}$.

II. PROBLEM SETUP AND PRELIMINARIES

In this section the nonlinear, discrete-time optimal control setup investigated in the note is introduced. Then, we review two numerical methods for optimal control related to the proposed approach, discussed in [10] and in [11].

A. Discrete-time Optimal Control Setup

We consider nonlinear, discrete-time systems described by

$$x_{t+1} = f(x_t, u_t) \quad t \in \mathbb{N} \quad (1)$$

where $x_t \in \mathbb{R}^n$ and $u_t \in \mathbb{R}^m$ are the state and the input of the system at time t , respectively. The map $f : \mathbb{R}^n \times \mathbb{R}^m \rightarrow \mathbb{R}^n$ is the vector field describing the nonlinear dynamics. The initial condition of the system is a fixed value $x_{\text{init}} \in \mathbb{R}^n$.

For notational convenience, we use $\mathbf{x} \in \mathbb{R}^{nT}$ and $\mathbf{u} \in \mathbb{R}^{mT}$ to denote, respectively, the stack of the states x_t for all $t \in [1, T]$ and the inputs u_t for all $t \in [0, T - 1]$, that is $\mathbf{x} := \text{col}(x_1, \dots, x_T)$ and $\mathbf{u} := \text{col}(u_0, \dots, u_{T-1})$. Next we give a useful definition.

Definition 2.1 (Trajectory): A pair $(\mathbf{x}, \mathbf{u}) \in \mathbb{R}^{nT} \times \mathbb{R}^{mT}$ is called a *trajectory* of the system described by (1) if its components satisfy the constraint represented by the dynamics (1) for all $t \in [0, T - 1]$. In particular, \mathbf{x} is the state trajectory, while \mathbf{u} is the input trajectory. \square

Conversely, we refer to a generic pair $(\boldsymbol{\alpha}, \boldsymbol{\mu}) \in \mathbb{R}^{nT} \times \mathbb{R}^{mT}$ with $\boldsymbol{\alpha} := \text{col}(\alpha_1, \dots, \alpha_T)$ and $\boldsymbol{\mu} := \text{col}(\mu_0, \dots, \mu_{T-1})$ as a state-input *curve*, in analogy with the continuous-time terminology. Notice that a curve $(\boldsymbol{\alpha}, \boldsymbol{\mu})$ is not necessarily a trajectory, i.e., it does not necessarily satisfy the dynamics (1).

By rewriting the nonlinear dynamics (1) as an implicit equality constraint $h : \mathbb{R}^{nT} \times \mathbb{R}^{mT} \rightarrow \mathbb{R}^{nT}$ we define the trajectory manifold $\mathcal{T} \subset \mathbb{R}^{nT} \times \mathbb{R}^{mT}$ of (1) as the set $\mathcal{T} := \{(\mathbf{x}, \mathbf{u}) \mid h(\mathbf{x}, \mathbf{u}) = 0\}$. It can be shown that the tangent space to the trajectory manifold at a given trajectory (point), denoted as $T_{(\mathbf{x}, \mathbf{u})}\mathcal{T}$, is represented by the set of trajectories satisfying the linearization of the nonlinear dynamics $f(\cdot, \cdot)$ about the trajectory (\mathbf{x}, \mathbf{u}) .

Among all possible trajectories of system (1), we aim to optimize a given performance criterion defined over a fixed time horizon $[0, T]$. Formally, we look for a solution of the discrete-time optimal control problem

$$\min_{\mathbf{x} \in \mathbb{R}^{nT}, \mathbf{u} \in \mathbb{R}^{mT}} \sum_{t=0}^{T-1} \ell_t(x_t, u_t) + \ell_T(x_T) \quad (2a)$$

$$\text{subj. to } x_{t+1} = f(x_t, u_t), \quad t \in [0, T - 1] \quad (2b)$$

with initial condition $x_0 = x_{\text{init}} \in \mathbb{R}^n$, stage cost $\ell_t : \mathbb{R}^n \times \mathbb{R}^m \rightarrow \mathbb{R}$ and terminal cost $\ell_T : \mathbb{R}^n \rightarrow \mathbb{R}$.

Remark 2.2: For the sake of exposition, the algorithm presented in the paper is tailored for *unconstrained* optimal control problems, neglecting the presence of state-input constraints. However, constraints can be addressed by adopting barrier function approaches (e.g., [12]). Although these approaches may influence the numerical properties and performance of the algorithm, they have demonstrated successful results for Projection Operator-based algorithms in various settings (cf. the review paper [14] and references therein). \square

Assumption 2.3: All functions $\ell_t(\cdot, \cdot)$, $\ell_T(\cdot)$ and $f(\cdot, \cdot)$ are twice continuously differentiable, i.e., they are of class \mathcal{C}^2 . \square

Notice that, in light of the nonlinear equality constraint of the nonlinear dynamics, problem (2) is a nonconvex program.

Throughout the note, we will use the following shorthand notation for the linearization of both the cost function and dynamics about a generic trajectory $(\mathbf{x}^k, \mathbf{u}^k)$ at iteration $k > 0$

$$a_t^k := \nabla_{x_t} \ell_t(x_t^k, u_t^k), \quad b_t^k := \nabla_{u_t} \ell_t(x_t^k, u_t^k), \quad (3a)$$

$$A_t^k := \nabla_{x_t} f(x_t^k, u_t^k)^\top, \quad B_t^k := \nabla_{u_t} f(x_t^k, u_t^k)^\top. \quad (3b)$$

B. Gradient Method for Optimal Control

Next, we recall a numerical strategy proposed, e.g., in [10, Section 1.9] to solve a discrete-time optimal control problem as in (2) based on the gradient method.

The leading idea is to express the state x_t at each $t \in [0, T - 1]$ as a function of \mathbf{u} only. Formally, for all t we can introduce a map² $\phi_t : \mathbb{R}^{mT} \rightarrow \mathbb{R}^n$ such that $x_t := \phi_t(\mathbf{u})$, so that problem (2) can be recast into the reduced version

$$\min_{\mathbf{u}} \sum_{t=0}^{T-1} \ell_t(\phi_t(\mathbf{u}), u_t) + \ell_T(\phi_T(\mathbf{u})) = \min_{\mathbf{u}} J(\mathbf{u}) \quad (4)$$

where the optimization variable is only the input sequence $\mathbf{u} \in \mathbb{R}^{mT}$. Problem (4) is an unconstrained optimization problem in \mathbf{u} with a \mathcal{C}^2 cost function. Notice that the cost function $J(\mathbf{u})$ inherits from (2) its smoothness properties, but also its nonconvexity. Hence, problem (4) can be addressed via a gradient descent method in which each component u_t^k , $t \in [0, T - 1]$ of $\mathbf{u}^k \in \mathbb{R}^{mT}$ is iteratively updated as

$$u_t^{k+1} = u_t^k + \gamma^k \Delta u_t^k. \quad (5)$$

where $k > 0$ denotes the iteration counter, $\Delta u_t^k := \nabla_{u_t} J(\mathbf{u}^k)$, while the parameter $\gamma^k > 0$ is the so-called step-size.

The gradient of $J(\cdot)$ at every \mathbf{u}^k can be efficiently computed by properly exploiting a costate difference equation (to be simulated backward in time) based on the linearization of the cost and the system dynamics at a given trajectory $(\mathbf{x}^k, \mathbf{u}^k)$ according to (3). This backward pass reads, for each $k > 0$,

$$\lambda_t^k = A_t^{k\top} \lambda_{t+1}^k + a_t^k \quad (6a)$$

²Formally, the shooting map depends also on the initial condition x_{init} . Being it fixed, for notational convenience we drop this dependence.

$$\Delta u_t^k = -B_t^{k\top} \lambda_{t+1}^k - b_t^k. \quad (6b)$$

As mentioned above, the update of the costate $\boldsymbol{\lambda}^k = \text{col}(\lambda_1^k, \dots, \lambda_T^k)$ involves the linearization of both the cost and the dynamics at the current input estimate \mathbf{u}^k and corresponding state \mathbf{x}^k (cf. (3)). Then, the component $\Delta u_t^k \in \mathbb{R}^m$ of the update (descent) direction in (5) is obtained via (6). The algorithm makes explicit use of the state sequence \mathbf{x}^k (associated to the current input estimate \mathbf{u}^k), which is obtained by forward simulation of the dynamics (2b) over the horizon $[0, T - 1]$, i.e., via

$$x_{t+1}^{k+1} = f(x_t^{k+1}, u_t^{k+1}) \quad (7)$$

with $x_0^{k+1} = x_{\text{init}}$, so that $(\mathbf{x}^{k+1}, \mathbf{u}^{k+1})$ is a trajectory.

Remark 2.4: We stress that, as follows from (7), each state trajectory \mathbf{x}^{k+1} is generated by an open-loop simulation of the dynamics, so that the method is not practically implementable for systems exhibiting unstable behaviors. \square

C. Discrete-time PRONTO

Along the lines of [16], we present a discrete-time version of the continuous-time optimal control algorithm PRONTO [11].

The key idea of PRONTO is to use a stabilizing feedback in an optimal control method to gain numerical stability, and to interpret such (tracking) controller as a projection operator that maps (state-input) curves into system trajectories. Given a state-input curve $(\boldsymbol{\alpha}, \boldsymbol{\mu})$, let us formally consider a nonlinear tracking system given by

$$u_t = \mu_t + K_t(\alpha_t - x_t), \quad x_{t+1} = f(x_t, u_t), \quad (8)$$

where $K_t \in \mathbb{R}^{n \times m}$ is a properly selected gain matrix.

Remark 2.5: The feedback gain K_t in (8) should ensure local stability about the current state-input trajectory. Among different alternatives, a possible choice could be a linear quadratic regulator involving the system linearization about the current trajectory. Also, one can use more advanced design approaches, e.g., linear parameter varying controllers [20]. \square

System (8) defines a nonlinear map, denoted by $\mathcal{P} : \mathbb{R}^{nT} \times \mathbb{R}^{mT} \rightarrow \mathcal{T}$ (with \mathcal{T} the trajectory manifold) such that

$$\begin{bmatrix} \boldsymbol{\alpha} \\ \boldsymbol{\mu} \end{bmatrix} \mapsto \begin{bmatrix} \mathbf{x} \\ \mathbf{u} \end{bmatrix} := \mathcal{P}(\boldsymbol{\alpha}, \boldsymbol{\mu}) = \begin{bmatrix} \phi(\boldsymbol{\alpha}, \boldsymbol{\mu}) \\ \psi(\boldsymbol{\alpha}, \boldsymbol{\mu}) \end{bmatrix}, \quad (9)$$

where $\phi(\boldsymbol{\alpha}, \boldsymbol{\mu})$ and $\psi(\boldsymbol{\alpha}, \boldsymbol{\mu})$ are the state and input components of $\mathcal{P}(\boldsymbol{\alpha}, \boldsymbol{\mu})$. \mathcal{P} is a *projection* since $(\mathbf{x}, \mathbf{u}) = \mathcal{P}(\boldsymbol{\alpha}, \boldsymbol{\mu})$.

Thanks to the projection operator, the optimal control problem (2) can be written as

$$\min_{\boldsymbol{\alpha}, \boldsymbol{\mu}} \ell(\phi(\boldsymbol{\alpha}, \boldsymbol{\mu}), \psi(\boldsymbol{\alpha}, \boldsymbol{\mu})). \quad (10)$$

Figure 1 provides a graphical interpretation of PRONTO. Specifically, PRONTO iteratively refines, for all $k > 0$, a tentative solution of problem (10) according to the update

$$\begin{bmatrix} \mathbf{x}^{k+1} \\ \mathbf{u}^{k+1} \end{bmatrix} = \mathcal{P} \left(\underbrace{\begin{bmatrix} \mathbf{x}^k \\ \mathbf{u}^k \end{bmatrix} + \gamma^k \begin{bmatrix} \Delta \mathbf{x}^k \\ \Delta \mathbf{u}^k \end{bmatrix}}_{(\boldsymbol{\alpha}^{k+1}, \boldsymbol{\mu}^{k+1})} \right), \quad (11)$$

where $\gamma^k \in (0, 1]$ is the step-size, while the update direction $(\Delta \mathbf{x}^k, \Delta \mathbf{u}^k) \in \mathbb{R}^{nT} \times \mathbb{R}^{mT}$ is obtained by minimizing a quadratic approximation of the cost in (10) over the tangent space $T_{(\mathbf{x}, \mathbf{u})}^k \mathcal{T}$ at the current trajectory $(\mathbf{x}^k, \mathbf{u}^k)$.

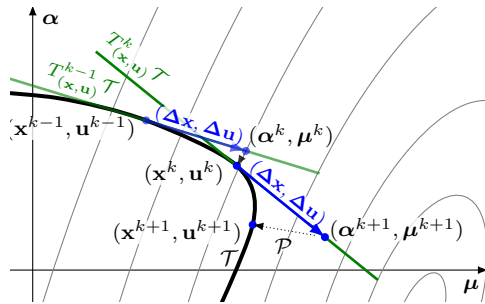


Fig. 1. Representation of PRONTO approach: in gray the level curves of the cost function $\ell(\cdot, \cdot)$, in black the trajectory manifold \mathcal{T} , in green the tangent space $T_{(\mathbf{x}, \mathbf{u})}^k \mathcal{T}$ about trajectory $(\mathbf{x}^k, \mathbf{u}^k)$. At each iteration k , the update direction $(\Delta \mathbf{x}, \Delta \mathbf{u})$ in blue is sought on the tangent space at the current trajectory $(\mathbf{x}^k, \mathbf{u}^k)$. The updated curve $(\boldsymbol{\alpha}^{k+1}, \boldsymbol{\mu}^{k+1})$ is then projected onto \mathcal{T} by the projection operator \mathcal{P} (dotted line).

The update direction $(\Delta \mathbf{x}^k, \Delta \mathbf{u}^k)$ is obtained as the minimizer of the following problem

$$\begin{aligned} \min_{(\Delta \mathbf{x}, \Delta \mathbf{u}) \in T_{(\mathbf{x}, \mathbf{u})}^k \mathcal{T}} & \nabla \ell(\mathbf{x}^k, \mathbf{u}^k)^\top \begin{bmatrix} \Delta x \\ \Delta u \end{bmatrix} \\ & + \frac{1}{2} \begin{bmatrix} \Delta x \\ \Delta u \end{bmatrix}^\top W(\mathbf{x}^k, \mathbf{u}^k) \begin{bmatrix} \Delta x \\ \Delta u \end{bmatrix}, \end{aligned} \quad (12)$$

where $W(\mathbf{x}^k, \mathbf{u}^k)$ is a square matrix. In the pure Newton version of PRONTO, $W(\mathbf{x}^k, \mathbf{u}^k)$ is the second order derivative of the reduced problem (10), including also second order derivatives of the projection operator, i.e.,

$$W(\mathbf{x}^k, \mathbf{u}^k) := \nabla^2 \ell(\mathbf{x}^k, \mathbf{u}^k) + \nabla^2 \mathcal{P}(\boldsymbol{\alpha}^k, \boldsymbol{\mu}^k) \nabla \ell(\mathbf{x}^k, \mathbf{u}^k) \quad (13)$$

We refer to [11] for a detailed discussion.

Remark 2.6: Depending on the choice of $W(\mathbf{x}^k, \mathbf{u}^k)$ some lower-order versions of PRONTO are possible, e.g., setting $W(\mathbf{x}^k, \mathbf{u}^k) = I$, with I being the identity matrix, we obtain a first-order method. Another possibility is to chose $W(\mathbf{x}^k, \mathbf{u}^k)$ as the second-order derivatives of the cost only. \square

It can be shown that the update direction $(\Delta \mathbf{x}^k, \Delta \mathbf{u}^k)$ is obtained solving the **Linear Quadratic (LQ) problem**

$$\begin{aligned} \min_{\Delta \mathbf{x}, \Delta \mathbf{u}} \sum_{t=0}^{T-1} & \left(\begin{bmatrix} a_t^k \\ b_t^k \end{bmatrix}^\top \begin{bmatrix} \Delta x_t \\ \Delta u_t \end{bmatrix} + \frac{1}{2} \begin{bmatrix} \Delta x_t \\ \Delta u_t \end{bmatrix}^\top \begin{bmatrix} Q_t^k & S_t^k \\ S_t^{k\top} & R_t^k \end{bmatrix} \begin{bmatrix} \Delta x_t \\ \Delta u_t \end{bmatrix} \right) \\ & + a_T^{k\top} \Delta x_T + \Delta x_T^\top Q_T^k \Delta x_T \\ \text{subj. to } & \Delta x_{t+1} = A_t^k \Delta x_t + B_t^k \Delta u_t, \quad t \in [0, T-1] \\ & \Delta x_0 = 0, \end{aligned} \quad (14)$$

where $Q_t^k \in \mathbb{R}^{n \times m}$, $S_t^k \in \mathbb{R}^{n \times m}$ and $R_t^k \in \mathbb{R}^{m \times m}$ are proper weight matrices, components of $W(\mathbf{x}^k, \mathbf{u}^k)$, while $A_t^k, B_t^k, a_t^k, b_t^k$ follow the shorthand notation in (3). Notice that in problem (14) a quadratic approximation of the cost of the reduced problem about the current iterate $(\mathbf{x}^k, \mathbf{u}^k)$ is considered and the computed update direction $(\Delta \mathbf{x}^k, \Delta \mathbf{u}^k)$ is constrained to the tangent space of current trajectory $(\mathbf{x}^k, \mathbf{u}^k)$, i.e., the set of trajectories satisfying the linearization of the nonlinear system dynamics $f(\cdot, \cdot)$ about $(\mathbf{x}^k, \mathbf{u}^k)$.

Algorithm 1 recaps the procedure described so far.

III. GoPRONTO

We are ready to present the main contribution of the note, namely a general set of first-order approaches, called GoPRONTO, for numerical optimal control. We start by describing a pure gradient (or steepest) descent implementation which we call Gradient GoPRONTO.

Algorithm 1 PRONTO

for $k = 0, 1, 2 \dots$ **do**
Step 1: compute descent direction $(\Delta \mathbf{x}^k, \Delta \mathbf{u}^k)$ by solving the **LQ problem** (14)

for $t = 0, \dots, T - 1$ **do**
Step 2: update (unfeasible) curve

$$\alpha_t^{k+1} = x_t^k + \gamma^k \Delta x_t^k, \quad \mu_t^{k+1} = u_t^k + \gamma^k \Delta u_t^k \quad (15)$$

Step 3: compute new (feasible) trajectory

$$u_t^{k+1} = \mu_t^{k+1} + K_t(\alpha_t^{k+1} - x_t^{k+1})$$

$$x_{t+1}^{k+1} = f(x_t^{k+1}, u_t^{k+1})$$

end for
end for

A. Derivation and Convergence of Gradient GoPRONTO

The founding idea of GoPRONTO is to formulate and solve an unconstrained optimization problem as done in the strategy shown in Section II-B. At the same time, we take also advantage from the beneficial effects of the state feedback of the projection operator (cf. (8) and (9)) used in Section II-C.

The proposed procedure is summarized in Algorithm 2, where we use the shorthand notation in (3) and we assume that, for all k , the state-input trajectory is initialized at $x_0^k = x_{\text{init}}$.

By comparing the steps (6) and (7) with (16) and (18) one can immediately recognize how the latter (Gradient GoPRONTO) is a closed-loop version of the former.

Specifically, by embedding the feedback system (8) (defining the projection operator) into the optimal control problem (2) one obtains the following optimal control problem

$$\min_{\mathbf{x}, \mathbf{u}, \alpha, \mu} \sum_{t=0} \ell_t(x_t, u_t) + \ell_T(x_T) \quad (19a)$$

$$\text{subj. to } x_{t+1} = f(x_t, u_t)$$

$$u_t = \mu_t + K_t(\alpha_t - x_t), \quad t \in [0, T - 1], \quad (19b)$$

$$x_0 = \alpha_0 = x_{\text{init}}.$$

In order to solve problem (19), we adopt the approach described in Section II-B. We recast

Algorithm 2 Gradient GoPRONTO

for $k = 0, 1, 2 \dots$ **do**

 set $\lambda_T^k = \nabla \ell_T(x_T^k)$
for $t = T - 1, \dots, 0$ **do**
Step 1: compute descent direction

$$\lambda_t^k = (A_t^k - B_t^k K_t)^{\top} \lambda_{t+1}^k + a_t^k - K_t^{\top} b_t^k \quad (16a)$$

$$\Delta \mu_t^k = -B_t^{k\top} \lambda_{t+1}^k - b_t^k \quad (16b)$$

$$\Delta \alpha_t^k = K_t^{\top} \Delta \mu_t^k \quad (16c)$$

end for
for $t = 0, \dots, T - 1$ **do**
Step 2: update (unfeasible) curve

$$\alpha_t^{k+1} = \alpha_t^k + \gamma^k \Delta \alpha_t^k, \quad \mu_t^{k+1} = \mu_t^k + \gamma^k \Delta \mu_t^k \quad (17)$$

Step 3: compute new (feasible) trajectory

$$u_t^{k+1} = \mu_t^{k+1} + K_t(\alpha_t^{k+1} - x_t^{k+1}) \quad (18)$$

$$x_{t+1}^{k+1} = f(x_t^{k+1}, u_t^{k+1})$$

end for
end for

problem (19) in its reduced form by expressing both the state x_t and the input u_t as functions of a state-input curve $(\boldsymbol{\alpha}, \boldsymbol{\mu})$ via two nonlinear maps

$$x_t = \phi_t(\boldsymbol{\alpha}, \boldsymbol{\mu}), \quad u_t = \psi_t(\boldsymbol{\alpha}, \boldsymbol{\mu}), \quad (20)$$

for all t . We notice that these maps can be seen as the closed-loop counterparts of $\phi_t(\mathbf{u})$ in Section II-B.³

³We make a slight abuse of notation by using the same symbol ϕ_t as in Section II-B. Again we omit the map dependence on the initial condition.

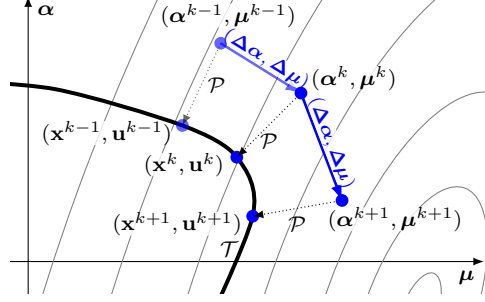


Fig. 2. Representation of GoPRONTO approach: in gray the level curves of the reduced cost $J(\cdot, \cdot)$, in black the trajectory manifold \mathcal{T} , in blue the descent directions. At each iteration k , the current curve (α^k, μ^k) is updated along the (generic) descent direction defined by the gradient of the reduced cost $J(\cdot, \cdot)$. The updated curve $(\alpha^{k+1}, \mu^{k+1})$ is, then, projected onto the trajectory manifold \mathcal{T} by the projection operator \mathcal{P} (dotted line).

Therefore, by exploiting (20), we can obtain a reduced instance of problem (2) given by

$$\begin{aligned} \min_{\alpha, \mu} \sum_{t=0}^{T-1} \ell_t(\phi_t(\alpha, \mu), \psi_t(\alpha, \mu)) + \ell_T(\phi_T(\alpha, \mu)) \\ = \min_{\alpha, \mu} J(\alpha, \mu), \end{aligned} \quad (21)$$

which is an unconstrained optimization problem in the variables $\alpha \in \mathbb{R}^{nT}$ and $\mu \in \mathbb{R}^{mT}$.

We point out that although the stacks of the maps in (20) correspond to the projection maps in (9), in the resolution of problem (21) we do not need to evaluate their derivatives.

Problem (21), similarly to its open-loop counterpart (4), is an unconstrained optimization problem with nonconvex, twice continuously differentiable cost function $J(\cdot, \cdot)$ (obtained as the composition of \mathcal{C}^2 functions). Therefore, we apply the gradient method in which the tentative solution (α^k, μ^k) is iteratively refined as

$$\alpha^{k+1} = \alpha^k - \gamma^k \nabla_{\alpha} J(\alpha^k, \mu^k), \quad \mu^{k+1} = \mu^k - \gamma^k \nabla_{\mu} J(\alpha^k, \mu^k)$$

where $k > 0$ is the iteration index while γ^k is the step-size. In parallel with Figure 1, a visual representation of this optimization problem is provided in Figure 2. We can see that the descent direction is searched in the entire space of curves (α, μ) (rather than on the tangent space to the trajectory manifold only). Moreover, the update-direction search is not restricted to any tangent space.

The curve update can be expressed also component-wise as

$$\alpha_t^{k+1} = \alpha_t^k - \underbrace{\gamma^k \nabla_{\alpha_t} J(\alpha^k, \mu^k)}_{-\Delta \alpha_t^k} \quad (22a)$$

$$\mu_t^{k+1} = \mu_t^k - \underbrace{\gamma^k \nabla_{\mu_t} J(\alpha^k, \mu^k)}_{-\Delta \mu_t^k} \quad (22b)$$

for all $t \in [0, T - 1]$, in which each pair $(\Delta\alpha_t^k, \Delta\mu_t^k) \in \mathbb{R}^n \times \mathbb{R}^m$ represents the descent direction in (16) computed by properly adapting the procedure detailed in Section II-B. As it can be seen in Figure 2, each (updated) state-input curve (α, μ) is then projected by the projection operator \mathcal{P} onto the trajectory manifold \mathcal{T} as per (18).

Next, we provide the convergence result for Algorithm 2, together with an assumption on the step-size.

Assumption 3.1: Let the step-size $\gamma^k \in \mathbb{R}$, $\gamma^k > 0$ be chosen via Armijo backtracking line search. □

Theorem 3.2: Let Assumptions 2.3 and 3.1 hold. Let $\{\alpha^k, \mu^k\}_{k \geq 0}$ be the sequence generated by Algorithm 2. Every limit point (α^*, μ^*) of the sequence $\{\alpha^k, \mu^k\}_{k \geq 0}$ satisfies $\nabla J(\alpha^*, \mu^*) = 0$. Moreover, let $(\mathbf{x}^*, \mathbf{u}^*)$ be the trajectory associated to state-input curve (α^*, μ^*) and λ^* the associated costate trajectory generated by Algorithm 2 in correspondence of (α^*, μ^*) . Then, $(\mathbf{x}^*, \mathbf{u}^*)$ represents a trajectory satisfying the first order necessary conditions for optimality in correspondence of costate trajectory λ^* . □

The proof of Theorem 3.2 can be found in [21].

Remark 3.3: Theorem 3.2 can be extended, with suitable assumptions, to different step-size selection rules e.g., constant step-size and diminishing step-size. □

B. Comparison with Inspiring Methods

In this subsection we detail the main differences among Algorithm 2 and the two existing, inspiring algorithms.

1) *Comparison with the gradient method presented in [10]:* GoPRONTO and the gradient method for optimal control (cf. Section II-B) share the same idea of the resolution of the optimal control problem via a gradient method in which the derivatives are computed through a costate dynamics. However, the introduction of the projection operator implies two fundamental improvements for GoPRONTO. First, we highlight that GoPRONTO enjoys numerical stability thanks to the different structure of the costate dynamics (16a). In fact, while the dynamical system represented by (6a) is governed by the matrix A_t^k , in our algorithm the adjoint system is governed by the matrix $A_t^k - B_t^k K_t$, which for a proper choice of the gain matrices K_t represents a stabilized, time-varying system as the horizon length goes to infinity. Moreover, thanks to the projection operator, in GoPRONTO the input trajectory \mathbf{u}^{k+1} implements a nonlinear tracking controller of the (updated) state-input curve $(\alpha^{k+1}, \mu^{k+1})$. Therefore, the trajectory update (18)

is performed under a closed-loop strategy rather than in open loop as in (7), so that dynamical systems subject to instability issues can be taken into account.

2) *Comparison with the PRONTO method presented in [11]*: GoPRONTO and PRONTO (cf. Section II-C) iteratively refine a state-input curve which is remapped, using the projection operator, into a state-input trajectory. An important difference relies on how these curves are calculated at each iteration. In PRONTO, see (15), the next state-input curve is obtained by perturbing the current trajectory with a descent direction obtained via an LQ problem. Therefore the direction is sought on the tangent space of the trajectory manifold at the current iterate. In GoPRONTO, instead, we proceed from curve to curve following the descent direction defined by the gradient of the reduced cost (cf. (22)) obtained through the adjoint system (16). Since no constraints are imposed on the descent direction and no LQ problems are solved to find the descent direction, a lower computation cost is in general required.

As a final remark, we point out that our algorithmic framework GoPRONTO can be exploited as a globalization technique for Newton's type optimization methods, see [10, Section 1.4] for a discussion.

IV. ACCELERATED VERSIONS OF GoPRONTO

In this section we show how the framework detailed in Section III can be combined with accelerated gradient-based optimization techniques available in the literature.

A. Conjugate GoPRONTO

The Conjugate GoPRONTO optimal control method is obtained by applying the Conjugate Gradient (CG) method to problem (21) (for further details about CG, see [22], [23]). Let, for all $k > 0$ and for all $t \in [0, T - 1]$,

$$\alpha_t^{k+1} = \alpha_t^k + \gamma^k \Delta \tilde{\alpha}_t^k, \quad \mu_t^{k+1} = \mu_t^k + \gamma^k \Delta \tilde{\mu}_t^k$$

where γ^k is chosen via Armijo backtracking line search, and the descent directions $\Delta \tilde{\alpha}_t^k$ and $\Delta \tilde{\mu}_t^k$ are obtained according to the CG algorithm as

$$\Delta \tilde{\alpha}_t^k := \Delta \alpha_t^k + \rho_{\alpha_t}^k \Delta \tilde{\alpha}_t^{k-1}, \quad \Delta \tilde{\mu}_t^k := \Delta \mu_t^k + \rho_{\mu_t}^k \Delta \tilde{\mu}_t^{k-1}$$

with $\rho_{\alpha_t}^k$ and $\rho_{\mu_t}^k$ defined as

$$\rho_{\alpha_t}^k := \frac{\Delta \alpha_t^k \top (\Delta \alpha_t^k - \Delta \alpha_t^{k-1})}{\|\Delta \alpha_t^{k-1}\|^2}, \quad \rho_{\mu_t}^k := \frac{\Delta \mu_t^k \top (\Delta \mu_t^k - \Delta \mu_t^{k-1})}{\|\Delta \mu_t^{k-1}\|^2}. \quad (23)$$

Algorithm 3 Conjugate GoPRONTO

for $k = 0, 1, 2 \dots$ **do**

for $t = T - 1, \dots, 0$ **do**

Step 1: compute descent direction $\Delta\alpha_t^k, \Delta\mu_t^k$ as in (16)

end for

for $t = 0, \dots, T - 1$ **do**

 compute $\rho_{\alpha_t}^k, \rho_{\mu_t}^k$ as in (23) and the update direction:

$$\Delta\tilde{\alpha}_t^k = \Delta\alpha_t^k + \rho_{\alpha_t}^k \Delta\tilde{\alpha}_t^{k-1} \qquad \Delta\tilde{\mu}_t^k = \Delta\mu_t^k + \rho_{\mu_t}^k \Delta\tilde{\mu}_t^{k-1}$$

Step 2: update (unfeasible) curve

$$\alpha_t^{k+1} = \alpha_t^k + \gamma^k \Delta\tilde{\alpha}_t^k, \qquad \mu_t^{k+1} = \mu_t^k + \gamma^k \Delta\tilde{\mu}_t^k$$

Step 3: compute new (feasible) trajectory via (18)

end for

end for

Recalling that $(\Delta\alpha_t^k, \Delta\mu_t^k)$ (cf. (22)) can be computed by means of (16), the procedure in Algorithm 3 is obtained.

As expected, when implemented with the necessary cautions, e.g., restarting policies and conjugacy tests, this method exhibits a faster convergence rate with respect to its plain gradient counterpart, see Section V for further details.

B. Heavy-Ball GoPRONTO

The Heavy-Ball GoPRONTO optimal control method is obtained by applying the Heavy-ball iteration (cf. [24]) to problem (21), i.e., for all $k > 0$ and for all $t \in [0, T - 1]$, we have

$$\begin{aligned} \alpha_t^{k+1} &= \alpha_t^k + \gamma^k \Delta\alpha_t^k + \gamma_{\text{HB}}(\alpha_t^k - \alpha_t^{k-1}) \\ \mu_t^{k+1} &= \mu_t^k + \gamma^k \Delta\mu_t^k + \gamma_{\text{HB}}(\mu_t^k - \mu_t^{k-1}), \end{aligned} \tag{24}$$

where $\gamma^k > 0$ and $\gamma_{\text{HB}} > 0$ are suitable step-sizes. The descent directions $\Delta\alpha_t^k, \Delta\mu_t^k$ are computed by means of the costate equation (16). Then, the updated curve obtained via (24) is projected into a new (feasible) trajectory via (18).

We point out that, although a faster convergence rate of the Heavy-Ball method (with respect to the plain gradient descent) is rigorously proved for convex problems only, the practical

implementation of this approach within our methodology confirmed these expectations (see Section V).

C. Nesterov's GoPRONTO

The Nesterov's GoPRONTO optimal control algorithm is obtained by applying Nesterov's iteration (cf. [25]) to problem (21). Let, for all $k > 0$ and for all $t \in [0, T - 1]$,

$$\alpha_t^{k+1} = \tilde{\alpha}_t^k + \gamma^k \Delta \tilde{\alpha}_t^k, \quad \mu_t^{k+1} = \tilde{\mu}_t^k + \gamma^k \Delta \tilde{\mu}_t^k \quad (25)$$

where γ^k is the step-size, while $\Delta \tilde{\alpha}_t^k$ and $\Delta \tilde{\mu}_t^k$ represent the gradient of $J(\cdot, \cdot)$ evaluated about the curve $(\tilde{\alpha}^k, \tilde{\mu}^k)$ defined as the stack of

$$\tilde{\alpha}_t^k = \alpha_t^k + \frac{k}{k+3}(\alpha_t^k - \alpha_t^{k-1}), \quad \tilde{\mu}_t^k = \mu_t^k + \frac{k}{k+3}(\mu_t^k - \mu_t^{k-1}). \quad (26)$$

The procedure is summarized in Algorithm 4.

Algorithm 4 Nesterov's GoPRONTO

for $k = 0, 1, 2 \dots$ **do**

for $t = T - 1, \dots, 0$ **do**

Step 1: compute descent direction

$$\begin{aligned} \lambda_t^k &= \left(\tilde{A}_t^k - \tilde{B}_t^k K_t \right)^\top \lambda_{t+1}^k + \tilde{a}_t^k - K_t^\top \tilde{b}_t^k \\ \Delta \tilde{\mu}_t^k &= -\tilde{B}_t^{k\top} \lambda_{t+1}^k - \tilde{b}_t^k, \quad \Delta \tilde{\alpha}_t^k = K_t^\top \Delta \tilde{\mu}_t^k. \end{aligned} \quad (27)$$

end for

for $t = 0, \dots, T - 1$ **do**

 compute $\tilde{\alpha}_t^k, \tilde{\mu}_t^k$ as in (26)

Step 2: update (unfeasible) curve via (25)

Step 3: compute new (feasible) trajectory via (18)

end for

end for

We point out that the descent direction $(\Delta \tilde{\alpha}_t^k, \Delta \tilde{\mu}_t^k)$ in Algorithm 4 is computed at the current auxiliary curve $(\tilde{\alpha}^k, \tilde{\mu}^k)$ rather than (α^k, μ^k) . In (27), in fact, the matrices $\tilde{A}_t^k, \tilde{B}_t^k, \tilde{a}_t^k, \tilde{b}_t^k$ are defined as

$$\tilde{a}_t^k := \nabla_{x_t} \ell_t(\tilde{x}_t^k, \tilde{u}_t^k), \quad \tilde{b}_t^k := \nabla_{u_t} \ell_t(\tilde{x}_t^k, \tilde{u}_t^k),$$

$$\tilde{A}_t^k := \nabla_{x_t} f(\tilde{x}_t^k, \tilde{u}_t^k)^\top, \quad \tilde{B}_t^k := \nabla_{u_t} f(\tilde{x}_t^k, \tilde{u}_t^k)^\top,$$

with $(\tilde{x}_t^k, \tilde{u}_t^k) = (\phi_t(\tilde{\alpha}^k, \tilde{\mu}^k), \psi_t(\tilde{\alpha}^k, \tilde{\mu}^k))$ for all k and t .

V. SIMULATIONS

Next, we give explanatory simulations of the algorithms proposed in the previous sections on a large-scale system made by a train of N inverted pendulums on carts, depicted in Figure 3. The code is implemented in Python on a computer with 2 GHz Quad-Core Intel Core i5 and 16 GB RAM.

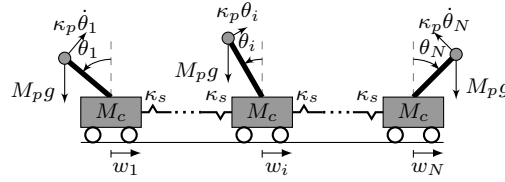


Fig. 3. Scheme of the train of inverted pendulum-on-cart systems.

1) *Simulation setup:* For each system $i \in \{1, \dots, N\}$, the nonlinear continuous-time dynamics is

$$\begin{aligned} M_p l^2 \ddot{\theta}_i + f_p \dot{\theta}_i - M_p l \sin(\theta_i) \ddot{w} - M_p l g \sin(\theta_i) &= 0 \\ (M_c + M_p) \ddot{w}_i + f_c \dot{w}_i - \frac{1}{2} M_p l \cos(\theta_i) \ddot{\theta}_i + \\ + \frac{1}{2} M_p l \sin(\theta_i) \dot{\theta}_i^2 - \kappa_s w_{i+1} + \kappa_s w_{i-1} &= u_i, \end{aligned}$$

where θ_i is the angle measured from the vertical upward position, w_i is the position of the cart and $g = 9.81 \text{ m/s}^2$. The control input is a force u_i applied to the cart. Table I reports the parameters for all the (identical) carts.

TABLE I
Pendulum-on-cart system parameters.

Pendulum			Cart		
Mass	M_p	0.2 [kg]	Mass	M_c	6.0 [kg]
Length	l	1.0 [m]	Spring Constant	κ_s	0.5 [$\frac{\text{N}}{\text{m}}$]
Damping	f_p	0.01 [$\frac{\text{Nms}}{\text{rad}}$]	Damping	f_c	10.0 [$\frac{\text{Ns}}{\text{m}}$]

The discrete-time dynamics, with state $x_{i,t} = (\theta_{i,t}, \dot{\theta}_{i,t}, w_{i,t}, \dot{w}_{i,t})^\top \in \mathbb{R}^4$ and input $u_{i,t} \in \mathbb{R}$ for all i is obtained via a Runge-Kutta integrator of order 4 with sampling period $\delta = 0.05$ seconds.

Thus, the state and the input of the entire system are defined as $x_t := \text{col}(x_{1,t}, \dots, x_{N,t}) \in \mathbb{R}^{4N}$ and $u_t := \text{col}(u_{1,t}, \dots, u_{N,t}) \in \mathbb{R}^N$. We aim at defining the optimal trajectory while tracking a reference curve. This curve tracking problem has a quadratic cost function where $\ell_t(x_t, u_t) = \|x_t - x_{\text{ref},t}\|_Q^2 + \|u_t - u_{\text{ref},t}\|_R^2$ and $\ell_T(x_T) = \|x_T - x_{\text{ref},T}\|_{Q_f}^2$ with symmetric, positive-definite matrices $Q := \text{diag}(Q_1, \dots, Q_N) \in \mathbb{R}^{4N \times 4N}$ and $R := \text{diag}(R_1, \dots, R_N)$ where, for all $i = 1, \dots, N$, $Q_i = \text{diag}(100, 1, 0.1, 0.1)$, $R_i = 0.1$. The terminal cost matrix Q_f is defined as the solution of the (discrete-time) algebraic Riccati equation evaluated at the linearization of the system about the equilibrium. We choose a feedback gain K_t in (19b) solving an LQ problem associated to the linearization of the dynamics about the trajectory $(\mathbf{x}^k, \mathbf{u}^k)$ available at the current iteration with quadratic cost matrices defined as $Q_{\text{reg}} = Q$, $R_{\text{reg}} = I$ and $Q_{f,\text{reg}} = Q_f$. The reference curve is defined, for each cart $i = 1, \dots, N$, as

$$\theta_{i,\text{ref}}(t) = \frac{\theta_{\text{amp}}^{\text{rad}} \tanh(t-T/2)(1-\tanh^2(t-T/2))}{\max_{t \in [0,T]} \theta_{\text{amp}}^{\text{rad}} \tanh(t-T/2)(1-\tanh^2(t-T/2))}$$

where $\theta_{\text{amp}}^{\text{rad}}$ represent the desired amplitude in radians. The desired angular velocity is determined by differentiating the smooth curve $\theta_{i,\text{ref}}(t)$. The other reference signals are zero.

2) *Comparison with existing numerical methods:* In this subsection, we compare GoPRONTO and the SQP-based algorithms for optimal control based on qpOASES, qpDUNES, HPIPM and the first-order OSQP, available in, e.g., `acados` [7]. For all algorithms, we consider the same numerical formulation of the optimal control problem and discretization scheme described above for $N = 3, 50, 100$ systems. We aim at performing a swing maneuver between $\pm\theta_{\text{amp}}$, $\theta_{\text{amp}} \in \{60^\circ, 80^\circ\}$ along the smooth reference curve $\theta_{i,\text{ref}}(t)$ representing the angular reference signal for each θ_i . This scenario represents a challenging setting for numerical optimal control algorithms due to the large dimension of the decisions variables for the NLP. Moreover, for $\theta_{\text{amp}} = 80^\circ$, the problem is even more challenging since it represents an asymptotically ill-posed problem. We chose this specific setting to provide an insight about the possibilities offered by GoPRONTO, which aims at representing a valid alternative in particular scenarios (e.g., quasi ill-posed problems and large-scale systems) where other approaches may face challenge. We remark the fact that GoPRONTO is implemented as in Algorithm 2 without pre-conditioning nor code optimization. The stepsize is selected via Armijo-line search and the shooting nodes coincide with the discretization time steps. The initial trajectory is $\theta_{i,t} \equiv 0$, $\dot{\theta}_{i,t} \equiv 0$, $w_{i,t} \equiv 0$, $\dot{w}_{i,t} \equiv 0$, for all t and i . The reference signals and the optimal trajectories obtained via GoPRONTO are shown in Figure 4 for the first of 100 pendulum-on-carts.

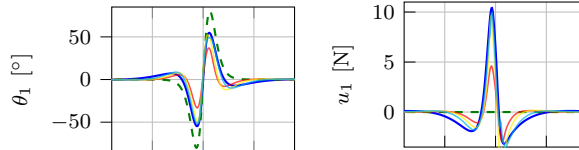


Fig. 4. Optimal angle and input trajectory obtained for the first pendulum-on-cart generated via GoPRONTO with $\theta_{\text{amp}} = 80^\circ$. In blue the optimal trajectory, in dashed green the reference signals. In red, yellow and cyan the trajectories at iteration $k = 0, 2, 4$, respectively.

The full condensing versions of qpOASES and HPIPM fail to provide a solution for all N for both references. This can be due to the fact that full condensing approaches eliminate state variables via the unstable dynamics. The partial condensing version of HPIPM, in which only few state variables are eliminated, successfully solves the problem for $N = 3, 50$ for both reference signals. Being HPIPM a second-order solver a faster convergence rate than GoPRONTO is achieved. A comparable convergence rate is achieved only with $\theta_{\text{amp}} = 80^\circ$ and $N = 50$. This can be due to the significant first-order acceleration required by the ill-posedness of the problem. For $N = 100$ HPIPM gives segmentation fault. As for partial condensing qpDUNES, it never reaches convergence. Finally, we compare GoPRONTO with the first-order solver OSQP. OSQP has a slower convergence rate for $N = 3$ and $\theta_{\text{amp}} = 80^\circ$, while it has a faster convergence rate for $\theta_{\text{amp}} = 60^\circ$. In the other cases it fails to provide a solution. Table II summarizes the performances achieved by the solvers that succeeded in at least one task.

TABLE II
Iterations of Gradient GoPRONTO, partial condensing HPIPM
and OSQP (\times means failure).

N	SQP solvers				GoPRONTO	
	Partial HPIPM		First-order OSQP		60°	80°
θ_{amp}	60°	80°	60°	80°	60°	80°
3	8	9	14	50	30	34
50	14	43	\times	\times	35	39
100	\times	\times	\times	\times	40	42

3) *Comparison with inspiring methods:* Next, Gradient GoPRONTO is implemented on the previously presented setup with $N = 2$. In this case and in the following simulations, the swing maneuver is performed between $+30^\circ$ and -30° . Algorithm 2 is compared with the Gradient Method (cf. Sec. II-B) and the first-order version of PRONTO (cf. Sec. II-C). The step-size γ^k

is selected by Armijo line search rule. The evolution of the norm of the gradient $\nabla J(\boldsymbol{\alpha}^k, \boldsymbol{\mu}^k)$, is presented in Figure 5. Notice that the Gradient Method diverges after very few iterations, while the first-order version of PRONTO exhibits a slower convergence rate compared with Algorithm 2.

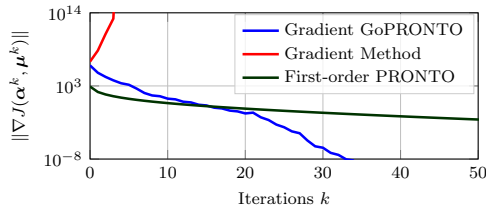


Fig. 5. Evolution of the norm of the gradient $\|\nabla J(\boldsymbol{\alpha}^k, \boldsymbol{\mu}^k)\|$ in Gradient GoPRONTO, the Gradient Method and PRONTO.

Table III compares GoPRONTO and PRONTO in terms of the computation time required to compute the descent direction and the total computation time with $N = 2, 3, 5, 10$. Since PRONTO computes the descent direction by solving an LQ problem, as the state-input dimensions increases, larger computation time per iteration is required with respect to GoPRONTO. In GoPRONTO, the total computation time includes the time required to compute the projection gain, which is recomputed only when it loses its stabilizing property, (2-3 times per simulation). While the total computation time is higher with low state dimension, GoPRONTO shows a faster convergence with high state dimensions. Notice that, in PRONTO, one could use the feedback gain obtained by solving the LQ problem at the price of losing the additional degree of freedom represented by the projection gain. It is worth mentioning that GoPRONTO is not a real-time control strategy at the moment, so these results do not provide a comprehensive evaluation of its performance on low-level hardware.

TABLE III

Computation times per iteration in [s].

Number of carts N	Computation time per iteration [s]				
	2	5	10	50	100
PRONTO	0.12	0.24	0.79	40.86	260.29
GoPRONTO	0.05	0.08	0.18	6.73	33.13
Total computation time [s]					
PRONTO	0.84	1.92	7.9	449.6	3123.48
GoPRONTO	1.76	3.36	9.28	328.63	1807.30

4) *Accelerated versions of GoPRONTO*: In the following, we compare Gradient GoPRONTO with its enhancements.

Comparison with Conjugate GoPRONTO: Here, $N = 2$ and the step-size γ^k is chosen via Armijo line search as required by the Conjugate Gradient method. Since the CG method is applied to a nonquadratic function, we need to deal with the resulting loss of conjugacy. The implemented method operates in cycles of conjugate direction steps, with the first step of each cycle being a basic gradient step. We choose to restart the policy when the conjugacy test fails, i.e. as soon as $|\nabla J(\alpha^{k+1}, \mu^{k+1})^\top \nabla J(\alpha^k, \mu^k)| > 0.7 \|\nabla J(\alpha^k, \mu^k)\|^2$. The evolution of the descent direction, i.e., the norm of the gradient $\nabla J(\alpha^k, \mu^k)$, is presented in Figure 6. We can see that the descent direction decreases with a faster rate when the CG-enhanced version is adopted.

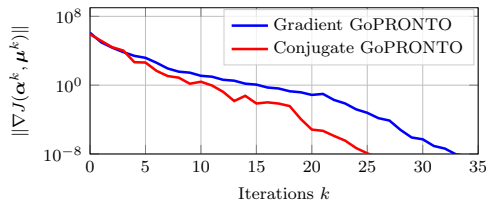


Fig. 6. Evolution of $\|\nabla J(\alpha^k, \mu^k)\|$ in Gradient GoPRONTO and Conjugate GoPRONTO for $N = 2$. γ^k is chosen via Armijo line-search.

Comparison with Heavy-Ball GoPRONTO and Nesterov's GoPRONTO: Finally, we consider $N = 50$ resulting in $x_t \in \mathbb{R}^{200}$ and $u_t \in \mathbb{R}^{50}$. The step-size γ^k is fixed with $\gamma^k \equiv \gamma = 10^{-3}$ while the Heavy-ball step $\gamma_{\text{HB}} = 0.5$. The evolution of the norm of the gradient $\nabla J(\alpha^k, \mu^k)$, is presented in Figure 7. Notice that the enhanced versions of GoPRONTO present a faster convergence rate than its basic implementation.

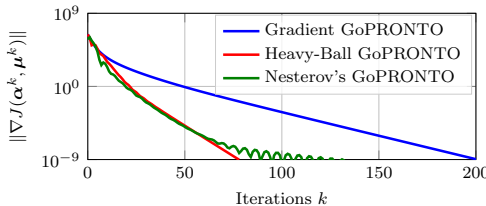


Fig. 7. Evolution of $\|\nabla J(\alpha^k, \mu^k)\|$ in Gradient GoPRONTO, Nesterov's GoPRONTO and Heavy-Ball GoPRONTO for $N = 50$. The stepsize is constant with $\gamma^k \equiv 10^{-3}$.

5) *Constrained optimal control:* In Figure 8 we present an example of optimal trajectory where input constraints are enforced. The problem setup is the same as above with $\theta_{\text{amp}} = 80^\circ$. For all carts, i.e., for all $i = 1, \dots, N$, the maximum input is saturated at $u_{\text{max}} = 5$ [N] $g(x_{i,t}) = \|u_{i,t}/u_{\text{max}}\| - 1 \geq 0$, for all $t = [0, T]$ added to the optimal control problem (2). This constraint is enforced via the barrier function approach proposed in [12].

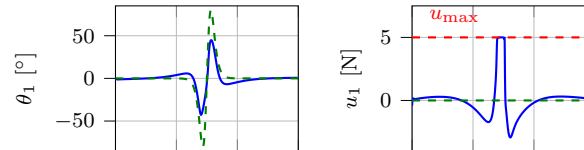


Fig. 8. Constrained optimal angle and cart position trajectory for the first pendulum-on-cart. In blue the optimal trajectory, in dashed green the reference trajectory, in dashed red the bound on the control action.

VI. CONCLUSIONS

In this note we proposed GoPRONTO, a novel first-order optimal control methodology that, thanks to the introduction of a nonlinear tracking system, achieves numerical robustness and produces, at each iteration, a feasible trajectory for the system dynamics. Moreover, its simple update rule allowed us to also design several accelerated versions of the plain scheme.

REFERENCES

- [1] S. Spedicato and G. Notarstefano, “Cloud-assisted distributed nonlinear optimal control for dynamics over graph,” *IFAC-PapersOnLine*, vol. 51, no. 23, pp. 361–366, 2018.
- [2] M. Diehl, H. J. Ferreau, and N. Haverbeke, “Efficient numerical methods for nonlinear mpc and moving horizon estimation,” in *Nonlinear model predictive control*. Springer, 2009, pp. 391–417.
- [3] S. J. Wright, *Primal-dual interior-point methods*. SIAM, 1997.
- [4] S. Boyd and L. Vandenberghe, *Convex Optimization*. Cambridge University Press, 2004.
- [5] B. Houska, H. J. Ferreau, and M. Diehl, “Acado toolkit—an open-source framework for automatic control and dynamic optimization,” *Optimal Control Applications and Methods*, vol. 32, no. 3, pp. 298–312, 2011.
- [6] T. Englert, A. Völz, F. Mesmer, S. Rhein, and K. Graichen, “A software framework for embedded nonlinear model predictive control using a gradient-based augmented Lagrangian approach (GRAMPC),” *Optimization and Engineering*, vol. 20, no. 3, pp. 769–809, 2019.
- [7] R. Verschuere, G. Frison, D. Kouzoupis, J. Frey, N. v. Duijkeren, A. Zanelli, B. Novoselnik, T. Albin, R. Quirynen, and M. Diehl, “Acados—a modular open-source framework for fast embedded optimal control,” *Mathematical Programming Computation*, vol. 14, no. 1, pp. 147–183, 2022.
- [8] L. T. Biegler and V. M. Zavala, “Large-scale nonlinear programming using IPOPT: An integrating framework for enterprise-wide dynamic optimization,” *Computers & Chemical Engineering*, vol. 33, no. 3, pp. 575–582, 2009.
- [9] A. Zanelli, A. Domahidi, J. Jerez, and M. Morari, “Forces nlp: an efficient implementation of interior-point methods for multistage nonlinear nonconvex programs,” *International Journal of Control*, vol. 93, no. 1, pp. 13–29, 2020.
- [10] D. P. Bertsekas, *Nonlinear programming*. Athena Scientific, 1999.
- [11] J. Hauser, “A projection operator approach to the optimization of trajectory functionals,” *IFAC Proceedings Volumes*, vol. 35, no. 1, pp. 377–382, 2002.
- [12] J. Hauser and A. Saccon, “A barrier function method for the optimization of trajectory functionals with constraints,” in *IEEE Conference on Decision and Control (CDC)*, 2006, pp. 864–869.

- [13] A. Saccon, J. Hauser, and A. P. Aguiar, “Optimal control on lie groups: The projection operator approach,” *IEEE Transactions on Automatic Control*, vol. 58, no. 9, pp. 2230–2245, 2013.
- [14] A. P. Aguiar, F. A. Bayer, J. Hauser, A. J. Häusler, G. Notarstefano, A. M. Pascoal, A. Rucco, and A. Saccon, “Constrained optimal motion planning for autonomous vehicles using pronto,” in *Sensing and control for autonomous vehicles*. Springer, 2017, pp. 207–226.
- [15] M. Filo and B. Bamieh, “Function space approach for gradient descent in optimal control,” in *IEEE American Control Conference (ACC)*, 2018, pp. 3447–3453.
- [16] F. A. Bayer, G. Notarstefano, and F. Allgöwer, “A projected SQP method for nonlinear optimal control with quadratic convergence,” in *IEEE Conference on Decision and Control (CDC)*, 2013, pp. 6463–6468.
- [17] B. Kouvaritakis, J. A. Rossiter, and J. Schuurmans, “Efficient robust predictive control,” *IEEE Transactions on Automatic Control*, vol. 45, no. 8, pp. 1545–1549, 2000.
- [18] M. S. Aftab and J. A. Rossiter, “Pre-stabilised predictive functional control for open-loop unstable dynamic systems,” *IFAC-PapersOnLine*, vol. 54, no. 6, pp. 147–152, 2021.
- [19] D. Kouzoupis, R. Quirynen, B. Houska, and M. Diehl, “A block based ALADIN scheme for highly parallelizable direct optimal control,” in *IEEE American Control Conference (ACC)*, pp. 1124–1129.
- [20] S. Spedicato, S. Mahesh, and G. Notarstefano, “A sparse polytopic lpv controller for fully-distributed nonlinear optimal control,” in *2019 18th European Control Conference (ECC)*. IEEE, 2019, pp. 554–559.
- [21] L. Sforzi, S. Spedicato, I. Notarnicola, and G. Notarstefano, “Goprnto: a feedback-based framework for nonlinear optimal control,” *arXiv preprint arXiv:2108.13308*, 2021.
- [22] M. R. Hestenes, E. Stiefel *et al.*, “Methods of conjugate gradients for solving linear systems,” *Journal of research of the National Bureau of Standards*, vol. 49, no. 6, pp. 409–436, 1952.
- [23] W. W. Hager and H. Zhang, “A survey of nonlinear conjugate gradient methods,” *Pacific journal of Optimization*, vol. 2, no. 1, pp. 35–58, 2006.
- [24] B. T. Polyak, “Some methods of speeding up the convergence of iteration methods,” *USSR Computational Mathematics and Mathematical Physics*, vol. 4, no. 5, pp. 1–17, 1964.
- [25] Y. Nesterov, “A method for solving a convex programming problem with convergence rate $O(1/k^2)$,” in *Soviet Mathematics. Doklady*, vol. 27, no. 2, 1983, pp. 367–372.

APPENDIX A

PROOF OF THEOREM 3.2

The proof is arranged in two main parts. In the first part, we prove that any limit point $(\boldsymbol{\alpha}^*, \boldsymbol{\mu}^*)$ of the sequence $\{\boldsymbol{\alpha}^k, \boldsymbol{\mu}^k\}_{k \geq 0}$ generated by Algorithm 2 is a stationary point of the unconstrained problem (21), i.e., it satisfies $\nabla J(\boldsymbol{\alpha}^*, \boldsymbol{\mu}^*) = 0$. Specifically, we show that Algorithm 2 represents a gradient descent method applied to problem (21).

Let us prove that the descent direction computed in (16) is the gradient of $J(\cdot, \cdot)$ evaluated at the point $(\boldsymbol{\alpha}^k, \boldsymbol{\mu}^k)$. To this end let us express the nonlinear dynamics in (19b) as an implicit

equality constraint $\tilde{h} : \mathbb{R}^{nT} \times \mathbb{R}^{mT} \times \mathbb{R}^{nT} \times \mathbb{R}^{mT} \rightarrow \mathbb{R}^{nT+mT}$ defined as

$$\tilde{h}(\mathbf{x}, \mathbf{u}, \boldsymbol{\alpha}, \boldsymbol{\mu}) := \begin{bmatrix} f(x_0, u_0) - x_1 \\ \vdots \\ f(x_{T-1}, u_{T-1}) - x_T \\ \mu_0 + K_0(\alpha_0 - x_0) - u_0 \\ \vdots \\ \mu_{T-1} + K_{T-1}(\alpha_{T-1} - x_{T-1}) - u_{T-1} \end{bmatrix}. \quad (28)$$

We also provide the concise formulation of the cost function (2a)

$$\ell(\mathbf{x}, \mathbf{u}) := \sum_{t=0}^{T-1} \ell_t(x_t, u_t) + \ell_T(x_T). \quad (29)$$

Therefore, by means of (29), we can compactly recast problem (19) as

$$\begin{aligned} \min_{\mathbf{x}, \mathbf{u}, \boldsymbol{\alpha}, \boldsymbol{\mu}} \quad & \ell(\mathbf{x}, \mathbf{u}) \\ \text{subj. to} \quad & \tilde{h}(\mathbf{x}, \mathbf{u}, \boldsymbol{\alpha}, \boldsymbol{\mu}) = 0. \end{aligned} \quad (30)$$

Then we can introduce an auxiliary function⁴ associated to problem (30), say $\mathcal{L} : \mathbb{R}^{nT} \times \mathbb{R}^{mT} \times \mathbb{R}^{nT} \times \mathbb{R}^{mT} \times \mathbb{R}^{nT+mT} \rightarrow \mathbb{R}$, defined as

$$\mathcal{L}(\mathbf{x}, \mathbf{u}, \boldsymbol{\alpha}, \boldsymbol{\mu}, \boldsymbol{\lambda}) := \ell(\mathbf{x}, \mathbf{u}) + \tilde{h}(\mathbf{x}, \mathbf{u}, \boldsymbol{\alpha}, \boldsymbol{\mu})^\top \boldsymbol{\lambda} \quad (31)$$

where the (multiplier) vector $\boldsymbol{\lambda} \in \mathbb{R}^{nT+mT}$ is arranged as

$$\boldsymbol{\lambda} := \text{col}(\lambda_1, \dots, \lambda_T, \tilde{\lambda}_1, \dots, \tilde{\lambda}_T)$$

with each $\lambda_t \in \mathbb{R}^n$ and $\tilde{\lambda}_t \in \mathbb{R}^m$. By defining $\phi(\cdot)$ and $\psi(\cdot)$ as the vertical stack of the maps $\phi_t(\cdot)$ and $\psi_t(\cdot)$ (Cf. (20)), we can see that, by construction, for all $(\boldsymbol{\alpha}, \boldsymbol{\mu}) \in \mathbb{R}^{nT} \times \mathbb{R}^{mT}$ it holds

$$\tilde{h}(\phi(\boldsymbol{\alpha}, \boldsymbol{\mu}), \psi(\boldsymbol{\alpha}, \boldsymbol{\mu}), \boldsymbol{\alpha}, \boldsymbol{\mu}) = 0. \quad (32)$$

Since $J(\boldsymbol{\alpha}, \boldsymbol{\mu}) \equiv \ell(\phi(\boldsymbol{\alpha}, \boldsymbol{\mu}), \psi(\boldsymbol{\alpha}, \boldsymbol{\mu}))$ (Cf. (21) and (29)), the auxiliary function (31) enjoys the following property

$$\mathcal{L}(\phi(\boldsymbol{\alpha}, \boldsymbol{\mu}), \psi(\boldsymbol{\alpha}, \boldsymbol{\mu}), \boldsymbol{\alpha}, \boldsymbol{\mu}, \boldsymbol{\lambda}) = J(\boldsymbol{\alpha}, \boldsymbol{\mu}) \quad (33)$$

⁴It is evidently the Lagrangian function of problem (30). However, since we do not pursue a Lagrangian approach, we prefer not to use such nomenclature.

for all $(\boldsymbol{\alpha}, \boldsymbol{\mu})$ and for all $\boldsymbol{\lambda} \in \mathbb{R}^{nT+mT}$. Therefore, in this formulation we can think about $\boldsymbol{\lambda}$ as a parameter or a degree of freedom. As a consequence of (33), it also results

$$\nabla \mathcal{L}(\phi(\boldsymbol{\alpha}, \boldsymbol{\mu}), \psi(\boldsymbol{\alpha}, \boldsymbol{\mu}), \boldsymbol{\alpha}, \boldsymbol{\mu}, \boldsymbol{\lambda}) = \nabla J(\boldsymbol{\alpha}, \boldsymbol{\mu}) \quad (34)$$

for all $(\boldsymbol{\alpha}, \boldsymbol{\mu})$ and, again, for all $\boldsymbol{\lambda}$, where the gradient of $\mathcal{L}(\cdot)$ is meant to be calculated only with respect to $(\boldsymbol{\alpha}, \boldsymbol{\mu})$.

In the following, we exploit (34) together with the degree of freedom represented by $\boldsymbol{\lambda}$ in order to efficiently compute $\nabla J(\cdot, \cdot)$. In fact, we can write the two components of the gradient of $J(\cdot, \cdot)$ as

$$\begin{aligned} \nabla_{\boldsymbol{\alpha}} J(\boldsymbol{\alpha}, \boldsymbol{\mu}) &= \nabla_{\boldsymbol{\alpha}} \phi(\boldsymbol{\alpha}, \boldsymbol{\mu}) \underbrace{\nabla_{\mathbf{x}} \mathcal{L}(\phi(\boldsymbol{\alpha}, \boldsymbol{\mu}), \psi(\boldsymbol{\alpha}, \boldsymbol{\mu}), \boldsymbol{\alpha}, \boldsymbol{\mu}, \boldsymbol{\lambda})}_{\text{underlined}} \\ &\quad + \nabla_{\boldsymbol{\alpha}} \psi(\boldsymbol{\alpha}, \boldsymbol{\mu}) \underbrace{\nabla_{\mathbf{u}} \mathcal{L}(\phi(\boldsymbol{\alpha}, \boldsymbol{\mu}), \psi(\boldsymbol{\alpha}, \boldsymbol{\mu}), \boldsymbol{\alpha}, \boldsymbol{\mu}, \boldsymbol{\lambda})}_{\text{underlined}} \\ &\quad + \nabla_{\boldsymbol{\alpha}} \mathcal{L}(\phi(\boldsymbol{\alpha}, \boldsymbol{\mu}), \psi(\boldsymbol{\alpha}, \boldsymbol{\mu}), \boldsymbol{\alpha}, \boldsymbol{\mu}, \boldsymbol{\lambda}) \end{aligned}$$

and

$$\begin{aligned} \nabla_{\boldsymbol{\mu}} J(\boldsymbol{\alpha}, \boldsymbol{\mu}) &= \nabla_{\boldsymbol{\mu}} \phi(\boldsymbol{\alpha}, \boldsymbol{\mu}) \underbrace{\nabla_{\mathbf{x}} \mathcal{L}(\phi(\boldsymbol{\alpha}, \boldsymbol{\mu}), \psi(\boldsymbol{\alpha}, \boldsymbol{\mu}), \boldsymbol{\alpha}, \boldsymbol{\mu}, \boldsymbol{\lambda})}_{\text{underlined}} \\ &\quad + \nabla_{\boldsymbol{\mu}} \psi(\boldsymbol{\alpha}, \boldsymbol{\mu}) \underbrace{\nabla_{\mathbf{u}} \mathcal{L}(\phi(\boldsymbol{\alpha}, \boldsymbol{\mu}), \psi(\boldsymbol{\alpha}, \boldsymbol{\mu}), \boldsymbol{\alpha}, \boldsymbol{\mu}, \boldsymbol{\lambda})}_{\text{underlined}} \\ &\quad + \nabla_{\boldsymbol{\mu}} \mathcal{L}(\phi(\boldsymbol{\alpha}, \boldsymbol{\mu}), \psi(\boldsymbol{\alpha}, \boldsymbol{\mu}), \boldsymbol{\alpha}, \boldsymbol{\mu}, \boldsymbol{\lambda}). \end{aligned}$$

Both these expressions involve the calculation of $\nabla \phi(\cdot)$ and $\nabla \psi(\cdot)$ which may be difficult to compute. However, since (34) holds for any $\boldsymbol{\lambda}$, we set this degree of freedom to greatly simplify the previous formulas. In fact, the underlined terms $\nabla_{\mathbf{x}} \mathcal{L}(\cdot)$ and $\nabla_{\mathbf{u}} \mathcal{L}(\cdot)$ have the following peculiar structure

$$\begin{aligned} \nabla_{\mathbf{x}} \mathcal{L}(\cdot) &= \nabla_{\mathbf{x}} \ell(\phi(\boldsymbol{\alpha}, \boldsymbol{\mu}), \psi(\boldsymbol{\alpha}, \boldsymbol{\mu})) \\ &\quad + \nabla_{\mathbf{x}} \tilde{h}(\phi(\boldsymbol{\alpha}, \boldsymbol{\mu}), \psi(\boldsymbol{\alpha}, \boldsymbol{\mu}), \boldsymbol{\alpha}, \boldsymbol{\mu})^{\top} \boldsymbol{\lambda} \end{aligned} \quad (36a)$$

and

$$\begin{aligned} \nabla_{\mathbf{u}} \mathcal{L}(\cdot) &= \nabla_{\mathbf{u}} \ell(\phi(\boldsymbol{\alpha}, \boldsymbol{\mu}), \psi(\boldsymbol{\alpha}, \boldsymbol{\mu})) \\ &\quad + \nabla_{\mathbf{u}} \tilde{h}(\phi(\boldsymbol{\alpha}, \boldsymbol{\mu}), \psi(\boldsymbol{\alpha}, \boldsymbol{\mu}), \boldsymbol{\alpha}, \boldsymbol{\mu})^{\top} \boldsymbol{\lambda}. \end{aligned} \quad (36b)$$

Therefore, with a proper choice of $\boldsymbol{\lambda}$ we can annihilate (36). In fact, by choosing $\boldsymbol{\lambda} = \bar{\boldsymbol{\lambda}}$ such that

$$\begin{aligned} \nabla_{\mathbf{x}} \mathcal{L}(\phi(\boldsymbol{\alpha}, \boldsymbol{\mu}), \psi(\boldsymbol{\alpha}, \boldsymbol{\mu}), \boldsymbol{\alpha}, \boldsymbol{\mu}, \bar{\boldsymbol{\lambda}}) &= 0 \\ \nabla_{\mathbf{u}} \mathcal{L}(\phi(\boldsymbol{\alpha}, \boldsymbol{\mu}), \psi(\boldsymbol{\alpha}, \boldsymbol{\mu}), \boldsymbol{\alpha}, \boldsymbol{\mu}, \bar{\boldsymbol{\lambda}}) &= 0 \end{aligned}$$

i.e., by setting

$$\begin{aligned} \nabla_{\mathbf{x}}\ell(\phi(\boldsymbol{\alpha}, \boldsymbol{\mu}), \psi(\boldsymbol{\alpha}, \boldsymbol{\mu})) \\ + \nabla_{\mathbf{x}}\tilde{h}(\phi(\boldsymbol{\alpha}, \boldsymbol{\mu}), \psi(\boldsymbol{\alpha}, \boldsymbol{\mu}), \boldsymbol{\alpha}, \boldsymbol{\mu})^\top \bar{\boldsymbol{\lambda}} = 0 \end{aligned} \quad (37a)$$

$$\begin{aligned} \nabla_{\mathbf{u}}\ell(\phi(\boldsymbol{\alpha}, \boldsymbol{\mu}), \psi(\boldsymbol{\alpha}, \boldsymbol{\mu})) \\ + \nabla_{\mathbf{u}}\tilde{h}(\phi(\boldsymbol{\alpha}, \boldsymbol{\mu}), \psi(\boldsymbol{\alpha}, \boldsymbol{\mu}), \boldsymbol{\alpha}, \boldsymbol{\mu})^\top \bar{\boldsymbol{\lambda}} = 0, \end{aligned} \quad (37b)$$

both the terms involving $\nabla\phi(\cdot)$ and $\nabla\psi(\cdot)$ cancel out. Hence, the gradient components of $J(\cdot, \cdot)$ reduces to

$$\begin{aligned} \nabla_{\boldsymbol{\alpha}}J(\boldsymbol{\alpha}, \boldsymbol{\mu}) &= \nabla_{\boldsymbol{\alpha}}\mathcal{L}(\phi(\boldsymbol{\alpha}, \boldsymbol{\mu}), \psi(\boldsymbol{\alpha}, \boldsymbol{\mu}), \boldsymbol{\alpha}, \boldsymbol{\mu}, \bar{\boldsymbol{\lambda}}) \\ \nabla_{\boldsymbol{\mu}}J(\boldsymbol{\alpha}, \boldsymbol{\mu}) &= \nabla_{\boldsymbol{\mu}}\mathcal{L}(\phi(\boldsymbol{\alpha}, \boldsymbol{\mu}), \psi(\boldsymbol{\alpha}, \boldsymbol{\mu}), \boldsymbol{\alpha}, \boldsymbol{\mu}, \bar{\boldsymbol{\lambda}}). \end{aligned}$$

By using again the definition of $\mathcal{L}(\cdot)$, the latter terms can be written as

$$\begin{aligned} \nabla_{\boldsymbol{\alpha}}J(\boldsymbol{\alpha}, \boldsymbol{\mu}) &= \nabla_{\boldsymbol{\alpha}}\tilde{h}(\phi(\boldsymbol{\alpha}, \boldsymbol{\mu}), \psi(\boldsymbol{\alpha}, \boldsymbol{\mu}), \boldsymbol{\alpha}, \boldsymbol{\mu})^\top \bar{\boldsymbol{\lambda}} \\ \nabla_{\boldsymbol{\mu}}J(\boldsymbol{\alpha}, \boldsymbol{\mu}) &= \nabla_{\boldsymbol{\mu}}\tilde{h}(\phi(\boldsymbol{\alpha}, \boldsymbol{\mu}), \psi(\boldsymbol{\alpha}, \boldsymbol{\mu}), \boldsymbol{\alpha}, \boldsymbol{\mu})^\top \bar{\boldsymbol{\lambda}}. \end{aligned} \quad (38)$$

With this derivation at reach, let us now focus on the k -th iteration of Algorithm 2. In correspondence of the current state-input curve $(\boldsymbol{\alpha}^k, \boldsymbol{\mu}^k)$, which represents a tentative solution of problem (21), we can compute the vector

$$\boldsymbol{\lambda}^k := \text{col}(\lambda_1^k, \dots, \lambda_T^k, \tilde{\lambda}_1^k, \dots, \tilde{\lambda}_T^k)$$

such that (37) holds with $(\boldsymbol{\alpha}, \boldsymbol{\mu}) = (\boldsymbol{\alpha}^k, \boldsymbol{\mu}^k)$ and $\bar{\boldsymbol{\lambda}} = \boldsymbol{\lambda}^k$. Therefore, by recalling the definitions of $\ell(\cdot)$ and $\tilde{h}(\cdot)$ in (29) and (28) and since the functions $f(\cdot), \ell_t(\cdot), \ell_T(\cdot)$ are differentiable by Assumption 2.3, the components λ_t^k of $\boldsymbol{\lambda}^k$ need to satisfy

$$\nabla\ell_T(\phi_T(\boldsymbol{\alpha}^k, \boldsymbol{\mu}^k)) - \lambda_T^k = 0$$

and, for all $t \in [0, T-1]$,

$$a_t^k + A_t^{k\top} \lambda_{t+1}^k - \lambda_t^k - K_t^\top \tilde{\lambda}_t^k = 0$$

which descends from (37a). As for the components $\tilde{\lambda}_t^k$ of $\boldsymbol{\lambda}^k$, they need to be such that for all $t \in [0, T-1]$

$$b_t^k + B_t^{k\top} \lambda_{t+1}^k - \tilde{\lambda}_t^k = 0$$

which comes from (37b). More compactly, a vector $\boldsymbol{\lambda}^k \in \mathbb{R}^{nT+mT}$ such that for $\bar{\boldsymbol{\lambda}} = \boldsymbol{\lambda}^k$ (37) is satisfied for a given $(\boldsymbol{\alpha}^k, \boldsymbol{\mu}^k)$, can be obtained by backward simulation of the adjoint system dynamics

$$\begin{aligned}\lambda_t^k &= (A_t^k - B_t^k K_t)^{\top} \lambda_{t+1}^k + a_t^k - K_t^{\top} b_t^k \\ \tilde{\lambda}_t^k &= b_t^k + B_t^{k\top} \lambda_{t+1}^k\end{aligned}\tag{40}$$

with terminal condition $\lambda_T^k = \nabla \ell_T(\phi_T(\boldsymbol{\alpha}^k, \boldsymbol{\mu}^k))$. With a suitable $\boldsymbol{\lambda}^k$ at hand, we can now compute the gradient of $J(\cdot, \cdot)$ as in (38), with $(\boldsymbol{\alpha}, \boldsymbol{\mu}) = (\boldsymbol{\alpha}^k, \boldsymbol{\mu}^k)$ and $\bar{\boldsymbol{\lambda}} = \boldsymbol{\lambda}^k$. Considering a generic time instant t and recalling the structure of $\tilde{h}(\cdot)$ in (28), we have

$$\begin{aligned}\nabla_{\alpha_t} J(\boldsymbol{\alpha}^k, \boldsymbol{\mu}^k) &= K_t^{\top} \tilde{\lambda}_t^k \\ &= K_t^{\top} (b_t^k + B_t^{k\top} \lambda_{t+1}^k)\end{aligned}\tag{41a}$$

and

$$\begin{aligned}\nabla_{\mu_t} J(\boldsymbol{\alpha}^k, \boldsymbol{\mu}^k) &= \tilde{\lambda}_t^k \\ &= b_t^k + B_t^{k\top} \lambda_{t+1}^k\end{aligned}\tag{41b}$$

for all $t \in [0, T - 1]$. Comparing (16) in Algorithm 2 with (41), we can see that $\Delta\alpha_t^k, \Delta\mu_t^k$ in (16) must satisfy

$$\begin{aligned}\Delta\alpha_t^k &:= -\nabla_{\alpha_t} J(\boldsymbol{\alpha}^k, \boldsymbol{\mu}^k) \\ \Delta\mu_t^k &:= -\nabla_{\mu_t} J(\boldsymbol{\alpha}^k, \boldsymbol{\mu}^k).\end{aligned}$$

Therefore, we proved that Algorithm 2 tackles problem (21) via a gradient descent method. In light of Assumption 3.1 the step-size γ^k in (17) is selected according to the Armijo rule on the cost function $J(\boldsymbol{\alpha}, \boldsymbol{\mu})$. Therefore, we can conclude that every limit point $(\boldsymbol{\alpha}^*, \boldsymbol{\mu}^*)$ of $\{\boldsymbol{\alpha}^k, \boldsymbol{\mu}^k\}_{k \geq 0}$ is a stationary point of $J(\boldsymbol{\alpha}, \boldsymbol{\mu})$, i.e., $\nabla J(\boldsymbol{\alpha}^*, \boldsymbol{\mu}^*) = 0$. This completes the first part of the proof.

In the second part, we prove that the state-input trajectory $(\mathbf{x}^*, \mathbf{u}^*) = (\phi(\boldsymbol{\alpha}^*, \boldsymbol{\mu}^*), \psi(\boldsymbol{\alpha}^*, \boldsymbol{\mu}^*))$ together with the costate vectors $\boldsymbol{\lambda}^* \in \mathbb{R}^{nT}$ generated by Algorithm 2 in correspondence of $(\boldsymbol{\alpha}^*, \boldsymbol{\mu}^*)$, satisfies the first order necessary optimality conditions for the optimal control problem (2). To this end, let us introduce the Hamiltonian function of problem (2) given by

$$H_t(x_t, u_t, \lambda_{t+1}) := \ell_t(x_t, u_t) + f(x_t, u_t)^{\top} \lambda_{t+1}$$

and next we show that

$$\nabla_{u_t} H_t(x_t^*, u_t^*, \lambda_{t+1}^*) = 0$$

and

$$\lambda_t^* = \nabla_{x_t} H_t(x_t^*, u_t^*, \lambda_{t+1}^*) \quad (42)$$

with terminal condition $\lambda_T^* = \nabla \ell_T(x_T^*)$.

In light of the projection-operator step (18), the point $(\mathbf{x}^*, \mathbf{u}^*)$ satisfies the dynamics (2b) by construction, i.e., it is a trajectory.

Let us define the shorthand for the linearization of the cost and the dynamics about the trajectory $(\mathbf{x}^*, \mathbf{u}^*)$

$$a_t^* := \nabla_{x_t} \ell_t(x_t^*, u_t^*), \quad b_t^* := \nabla_{u_t} \ell_t(x_t^*, u_t^*), \quad (43a)$$

$$A_t^* := \nabla_{x_t} f(x_t^*, u_t^*)^\top, \quad B_t^* := \nabla_{u_t} f(x_t^*, u_t^*)^\top. \quad (43b)$$

Then, we can define $\boldsymbol{\lambda}^*$ as the stack of the costate vectors $\lambda_t^* \in \mathbb{R}^n$, obtained from the adjoint equation (16a) evaluated at $(\boldsymbol{\alpha}^*, \boldsymbol{\mu}^*)$, i.e., for all $t \in [T-1, 0]$

$$\lambda_t^* = \left(A_t^* - B_t^* K_t^* \right)^\top \lambda_{t+1}^* + a_t^* - K_t^{*\top} b_t^* \quad (44)$$

with terminal condition $\lambda_T^* = \nabla \ell_T(x_T^*)$. Equation (44) corresponds to the gradient with respect to x_t of the Hamiltonian evaluated along the trajectory $(\mathbf{x}^*, \mathbf{u}^*)$, i.e., the first order necessary condition for optimality (42) holds by construction.

Finally, with $\boldsymbol{\lambda}^*$ at hand, we can see that condition

$$\nabla_{u_t} H_t(x_t^*, u_t^*, \lambda_{t+1}^*) = 0$$

can be written as

$$\nabla_{u_t} H_t(x_t^*, u_t^*, \lambda_{t+1}^*) = b_t^* + B_t^{*\top} \lambda_{t+1}^* \quad (45)$$

which corresponds to v_t^k , the gradient of $J(\cdot, \cdot)$ in (41b) evaluated at $(\boldsymbol{\alpha}^*, \boldsymbol{\mu}^*)$. In light of the first part of the proof, this term is equal to zero. Therefore, the first order necessary conditions for optimality are satisfied by the trajectory $(\mathbf{x}^*, \mathbf{u}^*)$, thus concluding the proof.